AGU PUBLICATIONS

JGR

Journal of Geophysical Research: Space Physics

RESEARCH ARTICLE
10.1002/2015JA021142

Key Points:
- Basic properties of the near-Earth current sheet are presented
- Convincing evidence for a bifurcated current sheet is shown
- The current density can increase without a high solar wind pressure

Correspondence to:
M. Saito,
miho.saito@me.com

Citation:
Saito, M. (2015), THEMIS two-point measurements of the cross-tail current density: A thick bifurcated current sheet in the near-Earth plasma sheet, *J. Geophys. Res. Space Physics*, *120*, 6258–6275, doi:10.1002/2015JA021142.

Received 19 FEB 2015
Accepted 10 JUL 2015
Accepted article online 14 JUL 2015
Published online 15 AUG 2015

THEMIS two-point measurements of the cross-tail current density: A thick bifurcated current sheet in the near-Earth plasma sheet

Miho Saito[1]

[1]Earth and Planetary Sciences, Tokyo Institute of Technology, Meguro, Japan

Abstract The basic properties of the near-Earth current sheet from 8 R_E to 12 R_E were determined based on Time History of Events and Macroscale Interactions during Substorms (THEMIS) observations from 2007 to 2013. Ampere's law was used to estimate the current density when the locations of two spacecraft were suitable for the calculation. A total of 3838 current density observations were obtained to study the vertical profile. For typical solar wind conditions, the current density near (off) the central plane of the current sheet ranged from 1 to 2 nA/m^2 (1 to 8 nA/m^2). All the high current densities appeared off the central plane of the current sheet, indicating the formation of a bifurcated current sheet structure when the current density increased above 2 nA/m^2. The median profile also showed a bifurcated structure, in which the half thickness was about 3 R_E. The distance between the peak of the current density and the central plane of the current sheet was 0.5 to 1 R_E. High current densities above 4 nA/m^2 were observed in some cases that occurred preferentially during substorms, but they also occurred in quiet times. In contrast to the commonly accepted picture, these high current densities can form without a high solar wind dynamic pressure. In addition, these high current densities can appear in two magnetic configurations: tail-like and dipolar structures. At least two mechanisms, magnetic flux depletion and new current system formation during the expansion phase, other than plasma sheet compression are responsible for the formation of the bifurcated current sheets.

1. Introduction

The cross-tail current sheet in the near-Earth tail plasma sheet, where hot high beta plasma dominates, supplies the precipitating particles that emit an aurora and act as a source for the high-energy particles in the inner magnetosphere. Their acceleration mechanisms are central issues in magnetosphere physics. The stability of the current sheet is of critical importance for substorm and acceleration mechanisms. Recently, a consensus was reached concerning the prebreakup arc and the initial brightening of auroral substorms originating from the near-Earth plasma sheet at a distance of 10 R_E [cf. *Donovan et al*., 2008; *Akasofu et al*., 2010; *Sergeev et al*., 2012]. *Akasofu* [2013] suggested that the magnetic energy inside this distance might account for auroral substorms. Some of the stored energy would be released by plasma instabilities [e.g., *Saito et al*., 2008], and as a result, these instabilities can lead to auroral development, particle acceleration, heating, and transport. The current sheet structure with minimum and maximum current densities may be related to the ground energy state and extra energy states of the magnetotail. The variability of the current density is a basic characteristic of the current sheet, and a comprehensive survey of this has not been reported so far.

The present study was motivated by recent observations from the Cluster and Time History of Events and Macroscale Interactions during Substorms (THEMIS) multispacecraft missions. *Saito et al*. [2011] examined a fortuitous event observed by THEMIS, in which all five spacecraft were located near each other in the near-Earth plasma sheet. This observation allowed them to examine a temporal change in the vertical profile of the current sheet during plasma sheet thinning and a gradual enhancement in the current density. Their observation indicated the formation of an inhomogeneous distribution in the current density, such as a bifurcated current sheet. For a simple one-dimensional current sheet where the integrated current increases proportionally with the square root of the lobe magnetic pressure, the current density increases with the lobe magnetic pressure and decreases with the thickness of the current sheet.

The conventional picture of thinning is that this occurs from a compression of the plasma sheet during the growth phase of a substorm. *Saito et al*. [2011] concluded differently that the enhancement of the

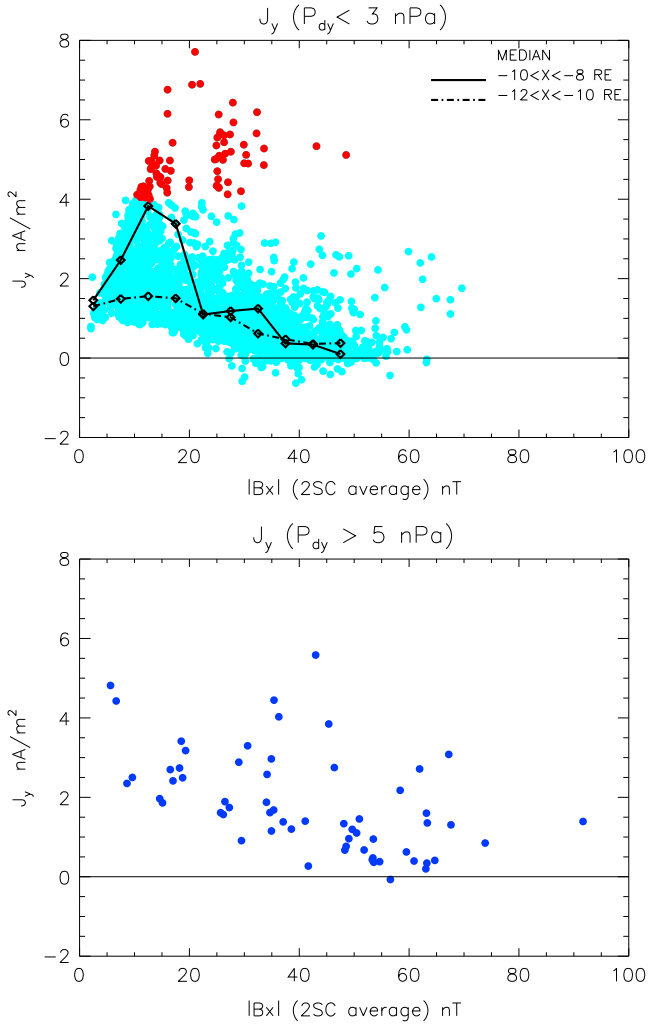

Figure 1. Vertical profiles of the cross-tail current density, J_y. (top) J_y versus the amplitude of B_x for a typical solar wind condition. High current densities ($J_y > 4$ nA/m^2) are denoted by the red filled circles; otherwise, the current densities are denoted by cyan filled circles. The black solid and black dashed lines show the median profile of the current density at $-8 > X > -10\,R_E$ and $-10 > X > -12\,R_E$, respectively. (bottom) J_y versus the amplitude of B_x for high solar wind pressure conditions.

lobe pressure was not associated with any plasma sheet thinning. This same feature was also confirmed in the midtail for several events by the Cluster spacecraft [*Snekvik et al.*, 2012]. *Saito et al.* [2011] showed that the current density increased to 8 nA/m^2, and they suggested that a current density with such a high value could not be distributed uniformly in the current sheet for the observed lobe pressure to sustain a force-balanced state. Therefore, they suggested that the current sheet would have to have a bifurcated structure, with two current density peaks located off the central plane of the current sheet. However, the spacecraft positions did not allow them to confirm that the current density near the central plane of the current sheet was lower than that off the central plane.

The presence of a bifurcated current sheet was initially indicated based on the ISEE 1 and 2 spacecraft observations at a distance of ~11 R_E by *Sergeev et al.* [1993]. They studied more than 10 events of the current sheet crossings and identified a thin embedded current sheet. The difference in B_x between the spacecraft indicated that the current density near the magnetic equatorial plane, $B_x \sim 0$, was not the highest. The Cluster observations in the midtail also indicated the presence of a bifurcated current sheet during a flapping motion [e.g., *Runov et al.*, 2003; *Sergeev et al.*, 2003], while *Tang et al.* [2006] reported a Cluster observation of a bifurcated current sheet with an absence of flapping motion during a quiet time. No conclusive evidence exists to relate flapping motion and formation of a bifurcated current sheet.

Previous studies have suggested that a bifurcated current in the midtail sheet was a feature that originated from the onset of magnetic reconnection [*Hoshino et al.*, 1996; *Thompson et al.*, 2006]. *Ricci et al.* [2004] modeled current sheet flapping, current sheet bifurcation, and magnetic reconnection consistently in a kinetic simulation as an evolution of a Harris current sheet. *Zelenyi et al.* [2002] have proposed an idea of plasma sheet "aging," where bifurcation appears during the late stage of current sheet thinning. These mechanisms are applicable to thin current sheet geometries, where ion demagnetization and/or Speiser-type orbits are important. The anisotropy of the ion temperature could be a cause for a bifurcated current sheet [*Cheng*, 1992; *Sitnov et al.*, 2003]. For both observational and theoretical reasons, the potential causes of a bifurcated current sheet in the near-Earth tail, where a typical plasma/current sheet is considerably thicker (say, a half thickness of 1 to 4 R_E), seem to be absent. In bifurcated current sheets, the scale length can be locally small at two locations in the current sheet. In contrast, a single peak current sheet has its minimum scale length located in the central plane of

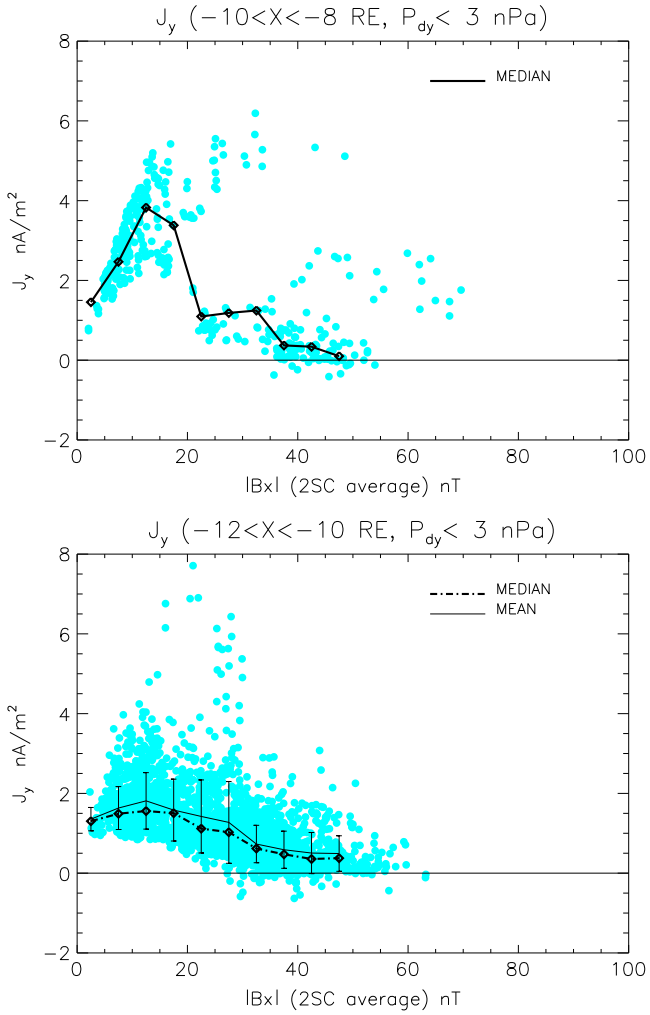

Figure 2. Vertical profiles of the cross-tail current density, J_y, for a typical solar wind condition (Figure 1, top) shown separately for $-8 > X > -10\,R_E$ and $-10 > X > -12\,R_E$.

the current sheet. *Delcourt et al.* [2004, 2006] have pointed out that such a difference is critical for the thermal ion dynamics in the magnetotail.

For a bifurcated (single peak) current sheet, charged particles with the adiabaticity parameter $\kappa \sim 1$ ($\kappa < 1$) behave quasi-adiabatically, where the square of κ is the ratio of the minimum radius of the magnetic field lines to the Larmor radius [*Büchner and Zelenyi*, 1989]. Quasi-adiabatic particles can experience a large energization when they encounter a region with a large curvature of the magnetic field lines, and as a result, they can turn into beams. Hence, the formation of a bifurcated current sheet may be closely related to energization and beam formation.

Another non-Harris current sheet is an embedded current sheet, which is a superposition of a thin, stronger current sheet on a thick, weaker current sheet. Both the thin and thick current sheets have their peak current densities in the central plane of the current sheet. An embedded current sheet has been reported from the Cluster data at a distance of 16–20 R_E [*Petrukovich et al.*, 2011, and references therein]. Petrukovich et al. suggested that the embedded current sheets might be formed by ions having Speiser-type trajectories or by anisotropic ions. *Asano et al.* [2005] tried to answer the question, "What type of structure is typical for current sheets in the magnetotail?" Although the answer to this question remains unknown, at least their results suggest that deviations from a Harris current sheet occur frequently.

The present paper focuses on the vertical structure of the current density in the near-Earth tail and its basic properties. This paper covers all geomagnetic conditions, whereas most previous studies have been concerned with the current sheet structure during substorms. Section 2 describes the data and method used, where simplifications are introduced to perform statistical analysis. Section 3 discusses the statistical variability and distribution of the current density. Section 4 shows that although this study assumes a number of simplifications in the analysis, the present results stand as convincing evidence that the current sheet is, on average, bifurcated as well as when the current density increases to high values. In section 5, conclusions and comments on future work are provided.

2. Data and Method

The present study used THEMIS [*Angelopoulos*, 2008] observations from 1 March 2007 to 31 December 2013. The THEMIS mission consisted of five identically instrumented spacecraft. The magnetic field data were obtained using fluxgate magnetometers [*Auster et al.*, 2008]. Solar Magnetic (SM) coordinates were used in the present analysis. Appendix A discusses why we chose SM coordinates rather than Geocentric Solar Magnetospheric (GSM)

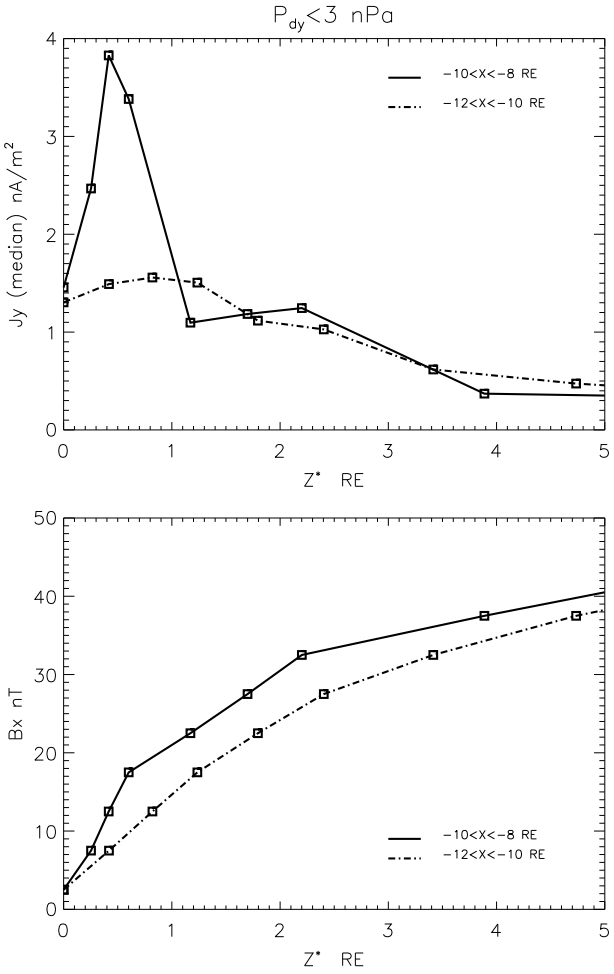

Figure 3. Median profiles of (top) J_y and (bottom) B_x as functions of Z at $-8 > X > -10\,R_E$ (solid line) and $-10 > X > -12\,R_E$ (dashed line).

coordinates for the region of interest. We have checked that the use of GSM coordinates did not change the statistical properties presented in the next section.

One method for calculating the cross-tail current density, J_y(see Appendix B), is to use simultaneous measurements of the magnetic field from two spacecraft, where Ampere's law can be approximated by

$$J_y = \frac{1}{\mu_0}\frac{\Delta B_x}{\Delta z}, \tag{1}$$

where ΔB_x and Δz are the differences in the magnetic field and the separation between two THEMIS spacecraft, respectively. Because the THEMIS orbits were not specifically designed to take spatial derivatives in the z direction, the observations needed to be selected carefully to minimize any potential errors. Equation (1) was used to obtain values for J_y when all the following criteria were satisfied:

1. The separation between two spacecraft in the z direction was $\Delta z < 0.7\ R_E$.
2. The ratio ${}^{\Delta z}/_{\Delta r}$ was > 2, where $\Delta r = \sqrt{\Delta x^2 + \Delta y^2}$ and is the radial separation of two spacecraft in the x-y plane.
3. ΔB_z was < 5 nT.

The first and second criteria were introduced to achieve high accuracy when performing spatial derivations in the z direction. While mathematically, the length of Δz needs to be infinitely small, in practice, Δz needs to be large enough to neglect any baseline differences between the magnetometers. For the THEMIS spacecraft, the spacing between the spacecraft was always large enough not to be of concern for these errors. Hence, only the upper limit was considered. The parameters in the first and second criteria were chosen by iteratively trying different values so that a set of observations was abundant enough to assess the vertical distribution. Owing to a finite length of Δz, the calculated current density was underestimated. Accordingly, the spatial profile obtained was less pronounced than the actual profile.

The third criterion was introduced for two reasons. First, the present method ignored the x dependence of ${\Delta B_z}/{\mu_0 \Delta x}$ in calculating J_y, and this component may not always be negligible in the near-Earth tail. Equation (1) was used with this criterion to avoid a large error. Accordingly, the ${\Delta B_z}/{\mu_0 \Delta x}$ component was small. At the most, the current density may have been overestimated by a maximum of ~2 nA/m^2 (e.g., $\Delta B_z = 80$ nT between $x = -6\ R_E$ and $-11\ R_E$). For a tail-like geometry, this value of ${\Delta B_z}/{\mu_0 \Delta x}$ should be much smaller. Second, this criterion was used to determine whether or not the coordinate system used was appropriate. A small value of ΔB_z is in accord with the assumption that the x axis of the SM coordinates is assumed to be parallel to the current sheet. In other words, the largest variance of the magnetic field is assumed to remain in the z direction. Note that the actual location of the central plane of the current sheet may lie somewhere between the $Z = 0$ plane of the GSM coordinates and that of the SM coordinates. The use of the third criterion meant that we only applied equation (1) when the central plane of the current sheet and the magnetic

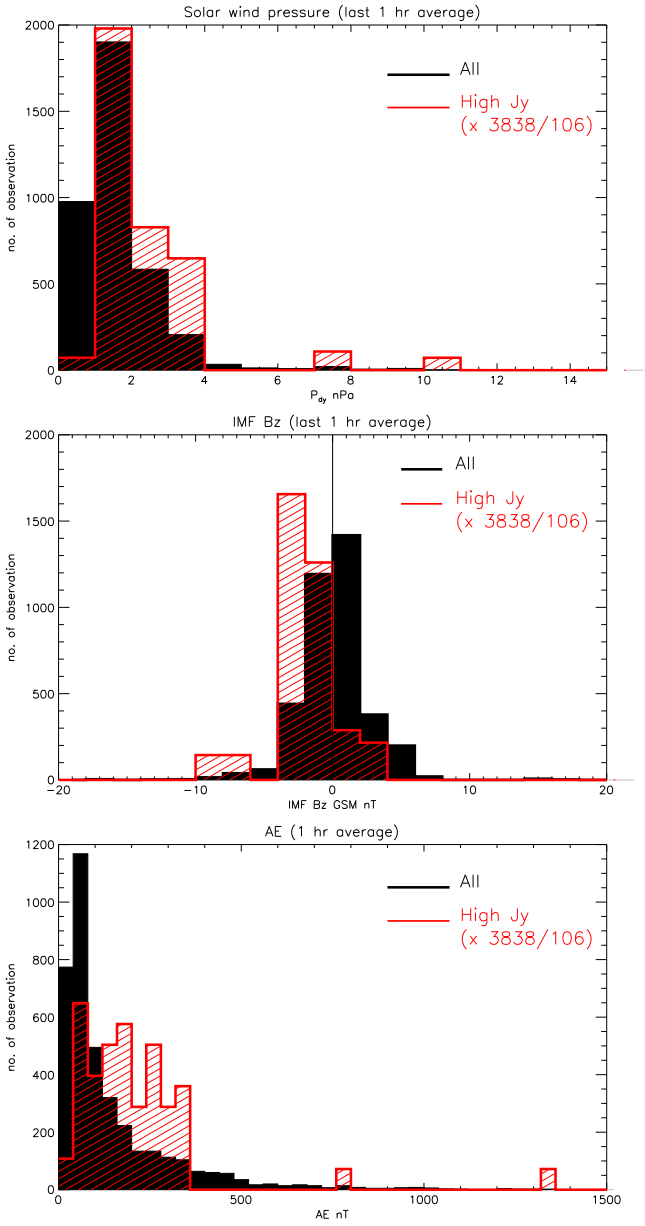

Figure 4. The dependence on the solar wind dynamic pressure, the interplanetary magnetic field of B_z, and the *AE* index for the occurrence of the high current densities. The red and black colored histograms denote the sets of high current density observations and the entire observations, respectively.

equator were approximately parallel to the $Z=0$ plane of the SM coordinates. See Appendix A for the orientation of the magnetic equator.

To focus on the vertical profile of the cross-tail current sheet, only the midnight sector ($|Y|<5\ R_E$) of the near-Earth magnetotail ($-8>X>-12\,R_E$) was examined. In addition, the observations were selected when the two spacecraft were in the same hemisphere. This criterion was checked using the sign of B_x and was required to determine the vertical location of the current density where the vertical location is given by the amplitude of B_x. A north-south symmetry was assumed throughout the present analysis. The average value of B_x between the two spacecraft was used to specify the vertical location. The magnetic field data were averaged for 5 min to eliminate fast temporal variations. The current density was sampled every 10 min to halve the number of observations to reduce any overlaps. As a result, we made 3838 current density observations for detailed analysis.

3. Results

Figure 1 shows observations of the current density, J_y, that satisfied all the selection criteria listed above. The values of J_y versus $|B_x|$ are presented separately for typical and high solar wind pressure conditions. This study used a 1 h average of the OMNI data to examine the solar wind dynamic pressure, P_{dy}, and we defined $P_{dy}<3$ nPa as a typical value and $P_{dy}>5$ nPa as a high solar wind pressure condition. Figure 1 includes 3464 observations of J_y for $P_{dy}<3$ nPa and 61 observations of J_y for $P_{dy}>5$ nPa. The remaining 313 observations of J_y for $5\geq P_{dy}\geq 3$ nPa are not shown here. Near the central plane (say for $|B_x|<20$ nT), the current density ranged from 1 to 8 nA/m^2 for $P_{dy}<3$ nPa and ranged from 2 to 6 nA/m^2 for $P_{dy}>5$ nPa. The variation in the current density turned out to be larger for typical solar wind conditions. It should be noted that the minimum current density did not reach a null value near the central plane for both solar wind conditions, showing a perpetual presence of the current sheet in the near-Earth tail. These two panels show that the minimum current density increased with the solar wind dynamic pressure. The increase in the minimum current density for high solar wind pressures can be explained by plasma sheet compression. If the current density is uniformly distributed, then a current density of ~1 nA/m^2 gives a half thickness of the current sheet of ~2.5 R_E for a lobe field amplitude of ~40 nT in a pressure-balanced state. When the solar wind dynamic pressure is high, the lobe field amplitude is also large. Hence, the increase in the minimum current density can be explained.

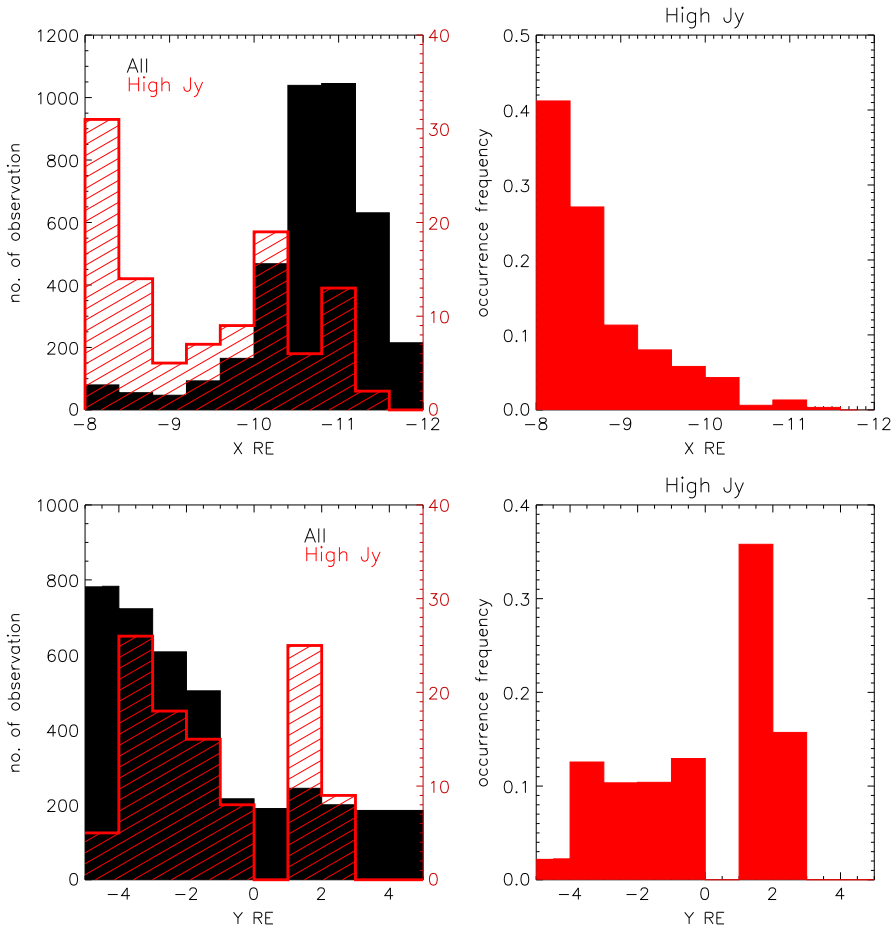

Figure 5. (left column) The dependences on the location, *X* and *Y*, for the occurrence of the high current densities. The red and black colored histograms denote the high current density observations and the entire observations, respectively. (right column) The normalized occurrence frequencies of the high current densities as a function of the location, *X* and *Y*.

On the other hand, the highest current densities cannot be simply explained by high solar wind pressures. They occur predominantly during typical solar wind conditions. For high solar wind pressure conditions, a current density $> 4\,\mathrm{nA/m^2}$ can form near the central plane of the current sheet, being consistent with the uniform compression of the plasma sheet. For typical solar wind conditions, there is no high current density near the central plane of the current sheet, and therefore, explanations of the high current density are outside the framework of plasma sheet compression.

The bifurcated structure of the cross-tail current sheet can be clearly observed in Figure 1 (top). The current density near the central plane of the current sheet showed a lesser variation ($1–2\,\mathrm{nA/m^2}$) compared with that ($1–8\,\mathrm{nA/m^2}$) slightly off the central plane, where $|B_x| \sim 20\,\mathrm{nT}$. The median vertical profiles were constructed using 392 and 3072 current density observations in two regions: $-8 > X > -10\,R_E$ and $-10 > X > -12\,R_E$, respectively. Both median profiles show that the peak of the current density is located off the central plane of the current sheet. On average, the degree of bifurcation is strong for the inner region $-8 > X > -10\,R_E$ but is weak for the outer region $-10 > X > -12\,R_E$. In Figure 2, the current densities in the two tail domains are plotted separately to clarify their differences.

Figure 3 shows the median J_y profile as a function of the location, *z*. The J_y profile as a function of $|B_x|$ (the median profiles in Figure 1, top) were rewritten by integrating

$$J_y(B_x) = \frac{1}{\mu_0}\frac{\Delta B_x}{\Delta z}. \tag{2}$$

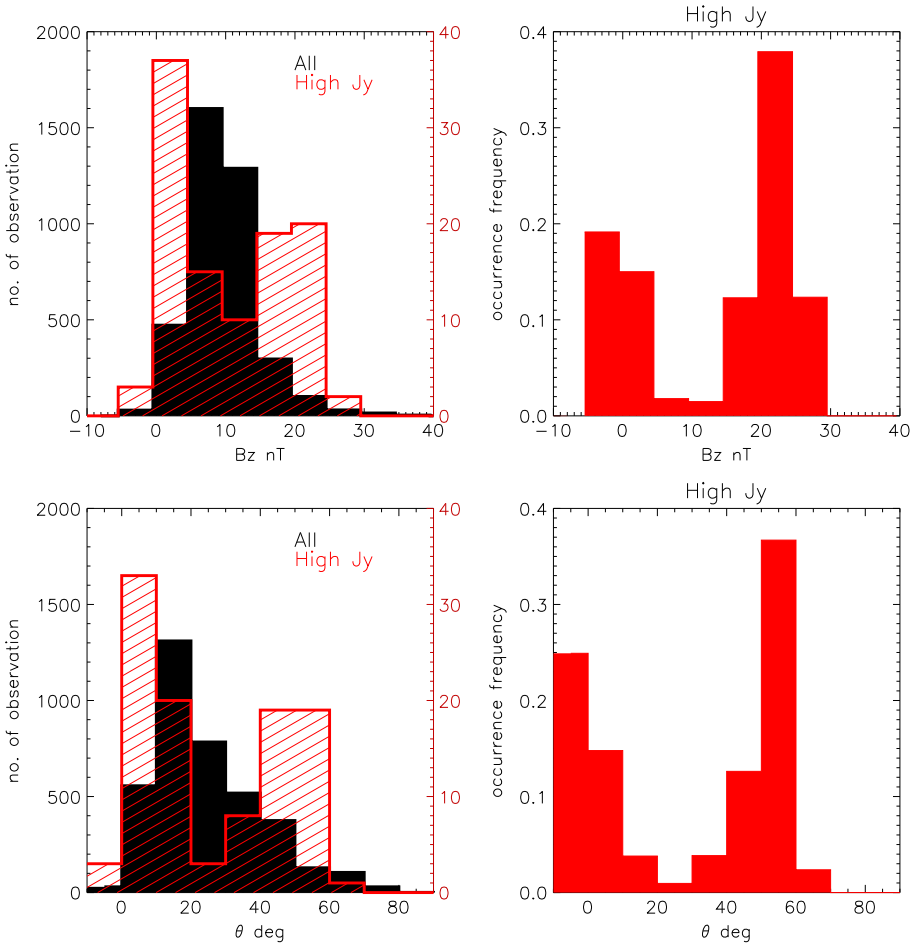

Figure 6. (left column) The dependence on the normal magnetic field, B_z, and the magnetic elevation angle for the occurrence of the high current densities. The colors denote the same as those defined in Figure 5. (right column) The normalized occurrence frequencies of the high current densities as a function of B_z and elevation angle.

Then, we have

$$z = \sum_{i=0} \Delta z(B_x) = \sum \frac{1}{\mu_0} \frac{\Delta B_x}{J_y(B_x)}. \tag{3}$$

Here B_x can be represented by an integer i.

$$B_x = \frac{\Delta B_x}{2} + i\Delta B_x. \tag{4}$$

In Figure 2, we used $\Delta B_x = 5$ nT to deduce the median profile. The location where $z = 0$ in Figure 3 corresponds to the location where $\Delta B_x = 2.5$ nT. Using equation (4), the median profile of $B_x(z)$ can also be reconstructed. Figure 3 shows that the median half thickness was about 3 R_E, while the difference between the peak of the current density and the central plane of the current sheet was 0.5 R_E and 1 R_E in regions $-8 > X > -10\,R_E$ and $-10 > X > -12\,R_E$, respectively.

To obtain further insight on the formation of bifurcated current sheets, the high current densities were examined statistically as follows. In the present study, we defined $J_y > 4\,\mathrm{nA/m^2}$ as a high current density observation. The probability of a high current density was found to be low, as there were only 106 occurrences out of 3838 observations. The high current density events occurred in a spatially and temporally limited window. Figure 4 shows the dependence of their occurrence on the solar wind dynamic pressure, B_z, of the interplanetary magnetic field (IMF) in GSM coordinates and the auroral

electrojet (*AE*) index. These dependencies are shown as two histograms to allow a comparison with the entire observations of J_y and the observations of high current densities. Being consistent with Figure 1, the solar wind dynamic pressure barely influenced the occurrence of high current densities. In contrast, the histograms of the IMF B_z and *AE* data for the high current density occurrences were different from those for the entire observations, indicating that a dependence existed. The average values of the southward component of the IMF B_z and *AE* were higher in the high current density observations. Hence, a high current density is a phenomenon that occurs prevalently in geomagnetically active events. The high current densities occurred in a consecutive time sequence and could be grouped into 21 intervals. Two intervals are shown in the appendix. To examine their association with substorms, we referred to the THEMIS data of field, particle, and ground-based auroral global images (http://themis.ssl.berkeley/edu/summary) and the time series data of geomagnetic indices from a substorm swift search (http://s-cubed). There were 14 substorm intervals out of 21 occurrences, including both growth and expansion phases. There were six intervals that were quiet times, while a single interval was unclassified.

Figure 5 shows the distributions of the locations, *X* and *Y*, for the entire observations, along with the high current density observations. Figure 5 (left column) is plotted using the same definitions as in Figure 4. The *X* and *Y* locations are the average values between the two spacecraft. Figure 5 (right column) shows the normalized occurrence frequency of the high current density observations as a function of the location. Most of the observations were sampled from the outer part, where $X \sim -11\,R_E$. The normalization showed that the occurrence frequency of high current densities was monotonically higher in the inner region of the tail. There was no noticeable dependence on the *Y* location.

Figure 6 shows the distribution of B_z and elevation angle, θ, of the magnetic field, where $\theta = \tan^{-1}\left(B_z/\sqrt{{B_x}^2 + {B_y}^2}\right)$. These were average values between the two spacecraft. Both parameters characterized the local magnetic geometry, such as the degree of stretched or tailed structure. The panels are organized using the same layout as defined in Figure 5. The histograms of B_z and θ for the entire observations show a single peaked distribution. However, the histograms for the high current density observations show a double peaked distribution. This characteristic is more emphasized in the normalized occurrence frequencies. These indicate that the formation of a high current density occurs in two magnetic geometries: in a tail-like structure (small B_z and small θ) and in a dipolar structure (large B_z and large θ). There are at least two different tail configurations that can support a high current density as well as the formation of a bifurcated current sheet.

4. Discussion

4.1. Analysis Techniques for the Current Sheet Structure

We examined the cross-tail current sheet and its vertical profile using two-point spacecraft measurements in the midnight sector ($|Y| < 5\ \ R_E$) of the near-Earth tail ($-8 > X > -12\,R_E$). The use of nearly 7 years THEMIS data allowed us to assess basic properties of the current sheet for the first time. The four-spacecraft Cluster mission has revealed a vertical profile of the tail current sheet by direct measurements during current sheet crossings and has shown the presence of a non-Harris current sheet [e.g., *Runov et al.*, 2003; *Asano et al.*, 2005; *Narita et al.*, 2013]. In these studies, the obtained current sheet structure was based on a limited number of event-based studies. In contrast, the present method is based on a relatively simple principle and, therefore, can be performed automatically for the extensive data set that covers various geomagnetic conditions. The assumptions of the pressure balance and the Harris current sheet profile are avoided. In addition, an association of spacecraft crossings of the current sheet and a flapping motion are not necessary. Because of this automated analysis, the vertical profile of the current density and its basic properties were revealed statistically. The statistical properties are useful for interpreting future improvements of in situ measurements of the current density to understand the current sheet structure. A high current density in the near-Earth tail means that the formation of a single thin current sheet for typical solar wind dynamic pressures is unlikely. Assuming that a Harris current sheet exists in the near-Earth tail will lead to a serious failure in an estimation of the thickness and the structure of the current sheet.

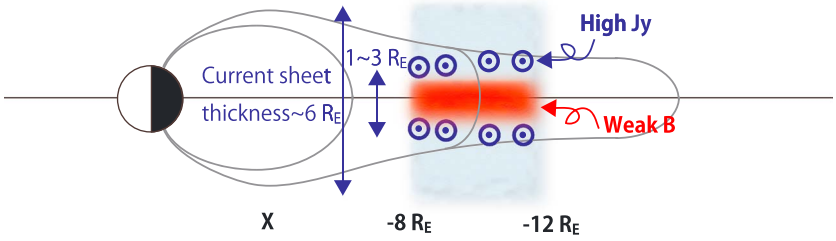

Figure 7. Illustration of the average current sheet profile.

A drawback of using THEMIS measurements is the large spacing between the spacecraft. The obtained current densities ranged from 0 to 8 nA/m^2. Some of the obtained current densities may be underestimated, while for a dipolar geometry, there are cases where the obtained current densities may be overestimated by up to ~2 nA/m^2, as explained in section 2. Accordingly, the structure of the obtained vertical profile may be less pronounced to some extent, and there may be a bias because of the fact that many current density observations satisfying the analysis criteria were obtained in 2010 and from the region $-10 > X > -12\,R_E$.

4.2. High Current Density

Because the geometry of the near-Earth tail can change widely from a tail-like to a dipolar structure, a large variation in current density may be expected to occur in the equatorial plane. However, the variation near the equatorial plane was found to be minor. The largest variation occurred slightly off the equatorial plane (0.5 to 1 R_E). These statistics suggest that the current sheet structure is bifurcated when the current density is >4 nA/m^2. We studied the scenario where a bifurcated current sheet was formed during the growth phase of substorms. This scenario has been supported by several observations. A generally accepted idea is that an enhanced current is a growth phase phenomenon [e.g., *Mitchell et al*., 1990; *Ohtani et al*., 1992]. The current density can increase with lobe pressure, which is another typical growth phase phenomenon [*Nagai et al*., 1997]. However, the present results only partly support this conventional view. The present study is relevant to an alternative process of plasma sheet thinning, for example, thinning caused by magnetic flux depletion as a result of dayside erosion of the magnetic flux [*Hsieh and Otto*, 2014]. Hsieh and Otto proposed that magnetic flux erosion in the dayside, which is a direct consequence of encountering the southward component of IMF, would lead to magnetic flux depletion in the inner edge of the tail plasma sheet. Their numerical model shows that the depletion of the magnetic flux can be another cause of plasma sheet thinning without an increase in lobe pressure. Their idea agrees well with our results, which show a relationship between the IMF B_z and a high current density in the tail. In addition, our study ruled out the notion that the solar wind dynamic pressure plays a major role in increasing the current density, but the solar wind dynamic pressure can raise the minimum possible value of the current density.

One unexpected finding was that a high current density stably forms structures with both tail-like and dipolar geometries. The dipolar geometry occurs during the expansion phase of a substorm. The occurrence of the expansion phase was confirmed from the THEMIS auroral and geomagnetic field data. A thinning of the plasma sheet is not the only way to explain the high current density and bifurcation of the current sheet. During dipolarization and substorm expansion phases, the magnetic field is substantially perturbed. Using a test particle simulation, *Greco et al*. [2002] have suggested that magnetic turbulence may explain the bifurcation of the current sheet. In their model, bifurcation was obtained by a weakening of the current density near the central plane of the current sheet from magnetic turbulence that perturbs the meandering motion v_y of ions.

4.3. Bifurcated Current Sheet and Diamagnetic Current

Figure 7 shows the average property of the near-Earth current sheet for a tail structure. Because the median profile shows a bifurcated structure, this bifurcated structure is a typical and stable structure. This fact suggests that the bifurcated structure may be stable against various instabilities such as fire hose instability and ballooning instability. Using both theory and simulations, *Matsui and Daughton* [2008]

suggested that the bifurcated current sheet has a stronger stabilizing effect on the tearing instability in the case of a thin current sheet. However, our results indicate that the average current sheet is thick. Matsui and Daughton's model may not be directly relevant to the near-Earth tail geometry.

The possible stability of bifurcated current sheets has been pointed out previously by *Génot et al*. [2005] based on Cluster observations. Note that the properties of the bifurcated current sheet from the Cluster data in the midtail differ from that in the near-Earth tail. While the current density in the equatorial plane does not reach a null value in the near-Earth tail, in the midtail it was found to be almost zero in the equatorial plane during bifurcation. This bifurcation was associated with small-scale neutral lines as reported by *Thompson et al*. [2006]. The vertical scale lengths were considerably different between the near-Earth tail and midtail regions, and particle effects are expected to be different. The midtail is often referred to as a site for magnetic reconnection and is characterized by a thin current sheet where electrons predominately carry the current. On the other hand, the current sheet is relatively thick in the near-Earth tail where the MHD approximation is worth considering.

The diamagnetic current $\boldsymbol{J}_\perp$ is given by

$$\boldsymbol{J}_\perp = \frac{\boldsymbol{B} \times \nabla P}{B^2}, \tag{5}$$

where P is the thermal plasma pressure, $\boldsymbol{B}$ is the magnetic field vector, and $B = |\boldsymbol{B}|$. For simplicity, $B_y = 0$. The y component of the diamagnetic current in the magnetic equatorial plane is

$$\boldsymbol{J}_{\perp y,\,\mathrm{eq}} = \frac{(\nabla P)_{x,\,\mathrm{eq}}}{B_{z,\mathrm{eq}}}. \tag{6}$$

The current density off the equatorial plane is

$$\boldsymbol{J}_{\perp y} = \frac{B_z(\nabla P)_x - B_x(\nabla P)_z}{{B_x}^2 + {B_z}^2}. \tag{7}$$

Equation (7) can be simplified by introducing α, where

$$\alpha = \frac{B_z}{B_x}. \tag{8}$$

This ratio is indicative of the magnetic elevation angle, having a value of about 0.2 for tail geometry and about 1 for dipolar geometry in the near-Earth tail. Note that the plasma pressure is constant along the magnetic field lines because the pressure balance along the magnetic field line may be easily and quickly achieved owing to the high temperature. Further, we have

$$\alpha = \frac{B_z}{B_x} \sim -\frac{(\nabla P)_x}{(\nabla P)_z}. \tag{9}$$

Then, equation (7) can be approximated as

$$\boldsymbol{J}_{\perp y} \sim \frac{\alpha B_x\{-\alpha(\nabla P)_z\} - B_x(\nabla P)_z}{{B_x}^2 + (\alpha B_x)^2} = -\frac{(\nabla P)_z}{B_x}. \tag{10}$$

Note that equation (10) is obtained without assuming $B_z = 0$. In the near-Earth tail, B_z is not negligible. To characterize the degree of bifurcation, we defined k as the ratio of current densities between the two points: the magnetic equator and the current density peak,

$$k \equiv \boldsymbol{J}_{\perp y} / \boldsymbol{J}_{\perp y,\,\mathrm{eq}}. \tag{11}$$

When k has a value of unity or less, the current sheet is either uniform or a single peaked profile along the z direction. When $k > 1$, the current sheet is bifurcated. From this observation, we have an average of $k \geq 1$ in the region $-10 > X > -12\,R_E$, and $k \sim 2$ in the region $-8 > X > -10\,R_E$. When the high current of 8 nA/m^2 appears off the equatorial plane, the value of k increases to 8. Substituting equations (6) and (10) into equation (11) gives

$$k = \frac{B_{z,\mathrm{eq}}}{B_x}\frac{L_{x,\mathrm{eq}}}{L_z}. \tag{12}$$

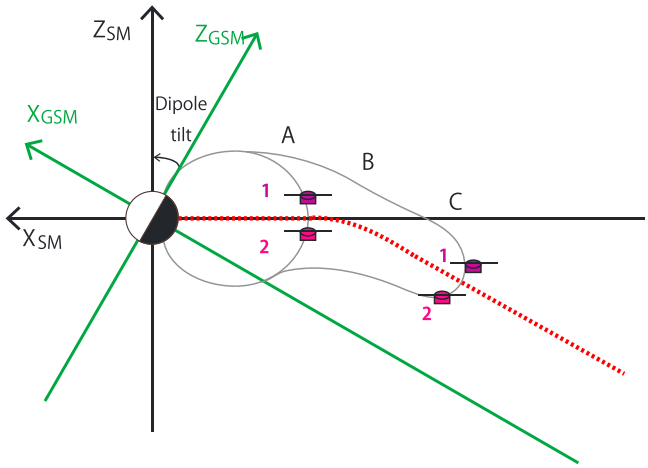

Figure A1. The idealistic orientation of the magnetic equatorial plane is shown by the red line. The actual orientation of the magnetic equator is shown in Figure A3 with a large dipole tilt angle.

The pressure gradients are replaced as $(\nabla P)_x = P/L_{x,eq}$, and $(\nabla P)_z = P/L_z$. Figure 1 shows that $|B_x|$ is about 20 nT at the peak of the current density profile. Figure 6 shows that there are two typical values of B_z for the occurrence of a high current density. In the following, we will consider two values of $B_{z,eq}$: $B_{z,eq} = 5$ nT and $B_{z,eq} = 20$ nT. For simplicity, we will let $L_{x,eq} = 5\,R_E$ and $1 < L_z < 4\,R_E$. When $B_{z,eq} = 5$ nT, we have $k \sim 0.3$ and 1.3 for $L_z = 4$ and $1\,R_E$, respectively. Hence, the thinning of the plasma sheet from 4 to $1\,R_E$ may account for the moderate bifurcation from a single peaked profile. The diamagnetic current and equation (12) can explain the average bifurcation for the outer region $-10 > X > -12\,R_E$. Note that L_z is the minimum scale of the gradient in the vertical direction. If L_z can decrease in the inner region $-8 > X > -10\,R_E$, then the bifurcation value of $k \sim 2$ can be obtained. Consideration beyond the isotropic MHD approximation may be needed to explain the bifurcated current sheet in the inner region $-8 > X > -10\,R_E$ for tail-like geometry. On the other hand, when $B_{z,eq} = 20$, large values of k can be easily obtained, such as $k \sim 1.3$ and 5 ($L_z = 4$ and $1\,R_E$, respectively). Moderate bifurcation can be easily achieved in a thick current sheet. However, assuming a small value, such as $L_z = 1\,R_E$, may be inconsistent with a large value of $B_{z,eq}$. In this respect, the diamagnetic current may explain only a weak to moderate bifurcation. In summary, this concise analysis suggests that the observed maximum bifurcation of $k \sim 8$ is difficult to explain solely by the diamagnetic current. Accordingly, the formation of a high current density is difficult to explain within isotropic MHD frameworks. Additional effects, such as anisotropy or particle effect may be important.

5. Conclusions

THEMIS observations from 2007 to 2013 allowed us to study the distribution of the cross-tail current density in the near-Earth tail ($-8 > X > -12\,R_E$). The statistical properties of the high current density observations are also presented for the first time. The statistical variation in the current density included minimum and maximum current densities that could occur under various geomagnetic conditions. The minimum possible current density with a nonzero value existing in the equatorial plane indicates a perpetual presence of the current sheet. In typical solar wind conditions, all the high current density observations were located off the central plane of the current sheet. By examining the median vertical profile, the current sheet was found to be thick and bifurcated. This bifurcated structure should be related to the stable state of the near-Earth tail. The average distance between the peak of the current density and the equatorial plane was 0.5 to $1\,R_E$. The average half thickness of the current sheet was approximately $3\,R_E$. Presumably, owing to this nonuniform profile, the current density can increase more than that expected from a uniform or single peaked profile. The high current density observations preferentially occurred during the growth phase and the expansion phase of substorms but also occurred in quiet times. Since the high current density observations are found to

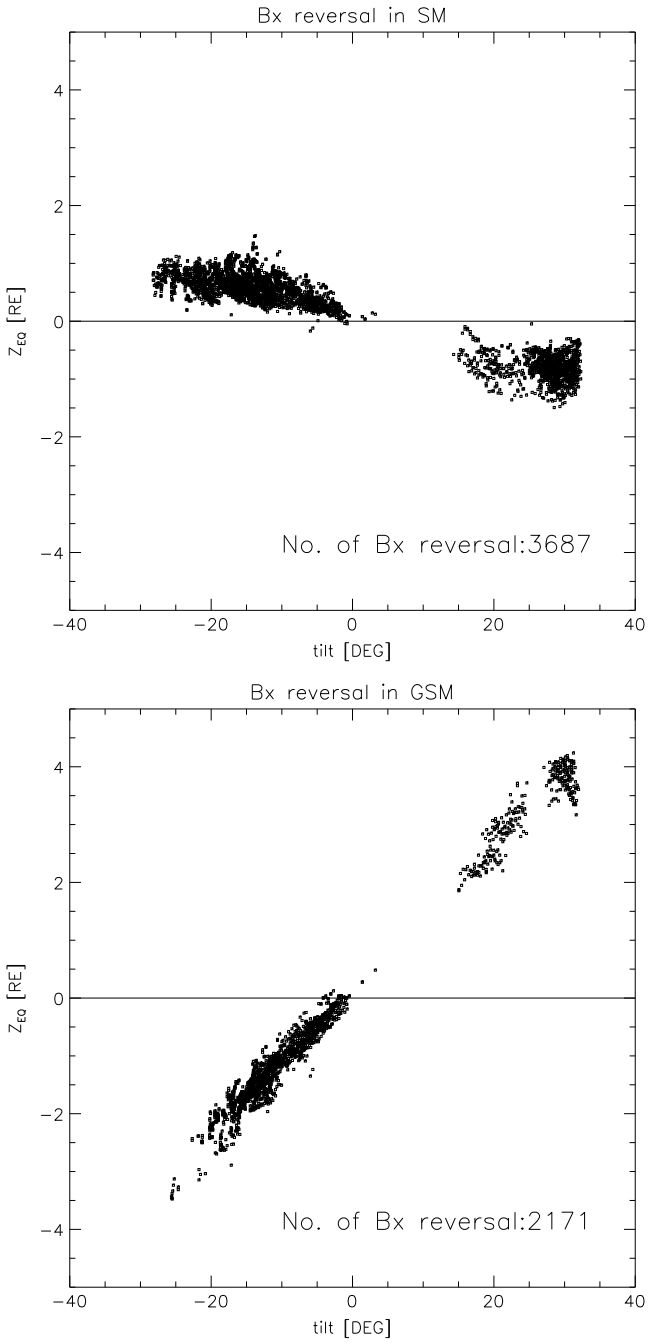

Figure A2. The locations of the B_x reversal versus dipole tilt angle.

be independent of the solar wind dynamic pressure, we concluded that the compression of the plasma sheet was not an explanation for the observed high current densities. Other mechanisms need to be developed to fully understand the structure and the evolution of the current sheet in the near-Earth tail. Compared with the solar wind dynamic pressure, the southward component of the interplanetary magnetic field controls the formation of high current densities in the near-Earth tail. Unconventional ideas and models, such as the tail evolution suggested by *Hsieh and Otto* [2014], are relevant to explain the present results.

Increased accuracy of the current density will be achieved in the future using multipoint spacecraft missions with smaller spacings, such as NASA's Magnetospheric Multiscale mission. The calculated current densities

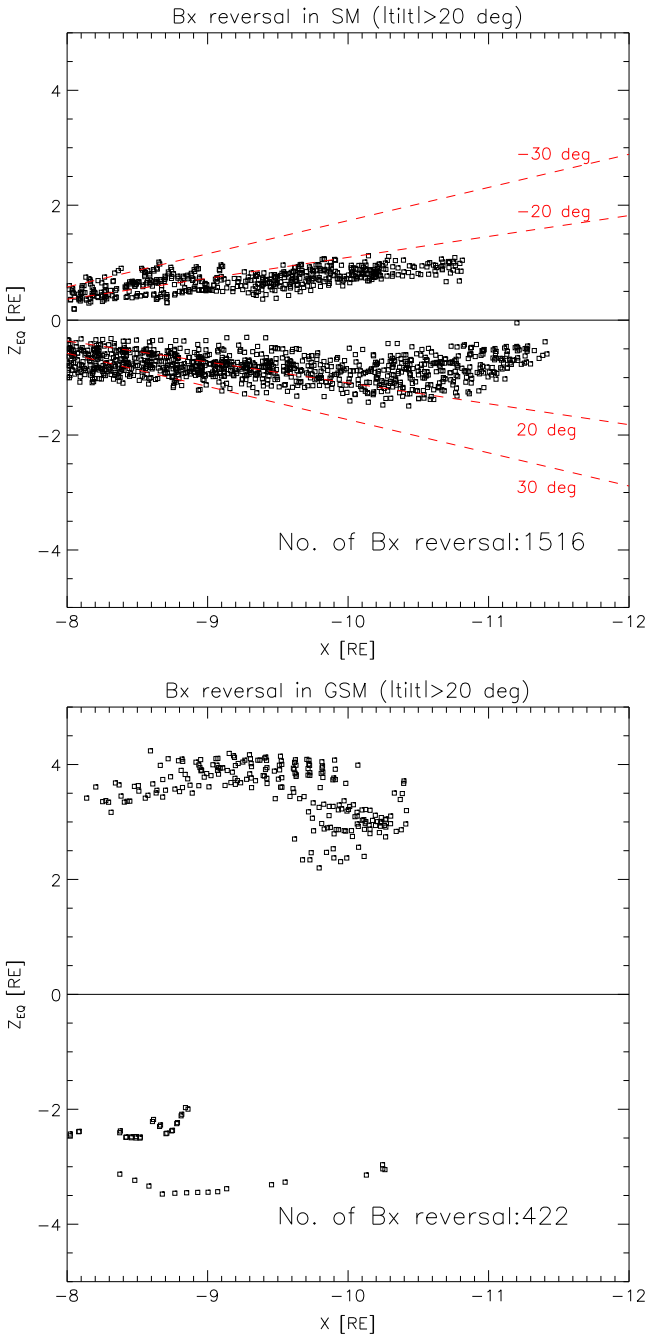

Figure A3. The locations of the B_x reversals versus position, x, indicating the orientation of the magnetic equator in the x-z plane with a dipole tilt angle $> 20°$. The red dotted lines denote the idealistic orientation of the magnetic equatorial plane. See text for details.

will be higher than those of the present method. In addition, the evaluation of the current density using particle measurements will increase the observations of high current densities. Although the present method underestimated the current density, the vertical profile was less pronounced, and our study presents convincing evidence of a bifurcated current sheet. We believe that the vertical profile obtained from the present analysis is useful for interpreting in situ current density data. High current density observations in the near-Earth tail are unlikely to be related to the formation of a single, thin current sheet but are related to a bifurcation of the current sheet.

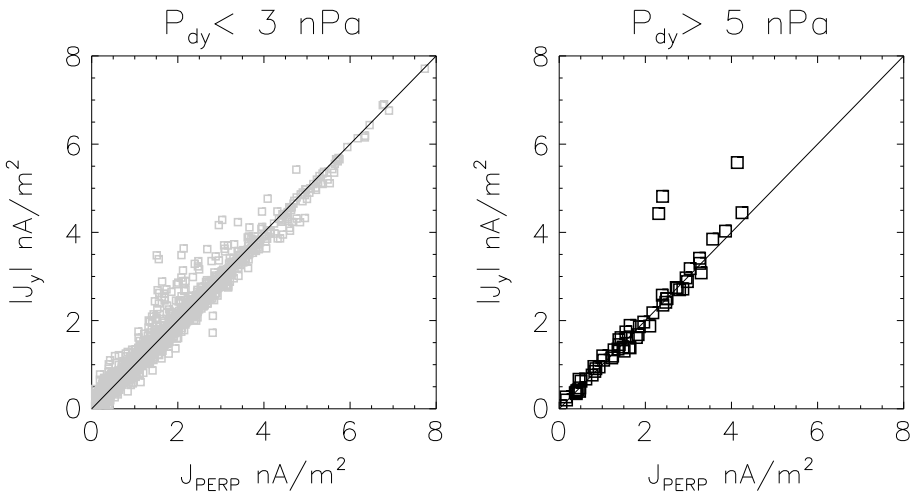

Figure A4. J_y versus $J_\perp$ for a typical solar wind condition of (left) $P_{dy} < 3$ nPa and high solar wind pressure (right) $P_{dy} > 5$ nPa. The solid lines indicate $J_y = J_\perp$.

Appendix A: Orientation of the Magnetic Equator

The choice of coordinate system, SM or GSM, is critical for studying the magnetic structure. This appendix will show that the SM coordinates are appropriate for the near-Earth tail ($X \sim -10\ R_E$). When the dipole tilt angle is zero, the SM and GSM coordinate systems are identical. When the dipole tilt angle is large, the magnetic equatorial plane hinges at an estimated distance of $7.4\ R_E$ to $10.4\ R_E$ [*Tsyganenko et al.*, 1998]. This problem is illustrated in Figure A1. The question is whether the near-Earth tail is a region denoted as B in Figure A1 where the plane of the magnetic equator is parallel to the x axis of the SM coordinates, denoted as A, or that of the GSM coordinates, denoted as C. We propose that this question can be answered by analyzing the number of magnetic field reversals. A reversal of B_x should indicate the location of the magnetic equatorial plane. The idea is that if the plane of the magnetic equator is not parallel to an axis of the chosen coordinate systems, then the detection of the magnetic equator based on a change in sign of B_x will fail for a large dipole tilt angle. For this purpose, we use 5 min averaged magnetic field data. The reversals in B_x were checked every 10 min, covering the entire period and all dipole tilt angles. We selected observations in which the separation in the z direction was $<1\ R_E$. The number of B_x reversals was 3687 using SM coordinates and 2171 using GSM coordinates. The use of the GSM coordinate system failed to identify some of the magnetic equators and, therefore, was not appropriate in the tail $-8 > X > -12\ R_E$ with a large dipole tilt angle.

Figure A2 shows the position of the magnetic equator as a function of the dipole tilt angle for both coordinate systems. Both plots show a dependence on the dipole tilt angle. The location Z_{EQ} is given by $Z_{EQ} = \left(Z_1 - Z_2 {}^{B_{x2}}/_{B_{x1}}\right) / \left(1 - {}^{B_{x2}}/_{B_{x1}}\right)$, where Z_1 and Z_2 are the positions of the two spacecraft and B_{x1} and B_{x2} are the x components of the magnetic field. The magnetic equators are distributed around the $Z = 0$ plane of the SM coordinates. As the dipole tilt angle increases, the magnetic equators become separated from the $Z = 0$ plane of the GSM coordinates. Knowing the location of the magnetic equator $Z_{EQ} = 4\ R_E$ with tilt angle = 30° in GSM coordinates, we obtained a hinging distance of $7\ R_E$ by fitting the results to the idealistic orientation of the magnetic equator, as shown in Figure A1.

Figure A3 shows the position of the magnetic equator as a function of the location, x, for dipole tilt angles >20°. The detected number of magnetic field reversals was significantly different between the SM and GSM data, confirming our proposition that detection using GSM coordinates failed notably for large dipole tilt angles. The idealistic orientations of the magnetic equator are plotted in Figure A3 for dipole tilt angles of ±20° and ±30°. We assumed a hinging distance of $7\ R_E$. If the idealistic orientation is correct, then the appropriate coordinate system would be the GSM coordinate system. However, we found that the GSM coordinates were not appropriate, because the orientation of the magnetic equator was different from the idealistic orientation, which has a sharp curve at the hinging distance. If the GSM coordinates are appropriate, then the location of the magnetic equator in SM coordinates should change

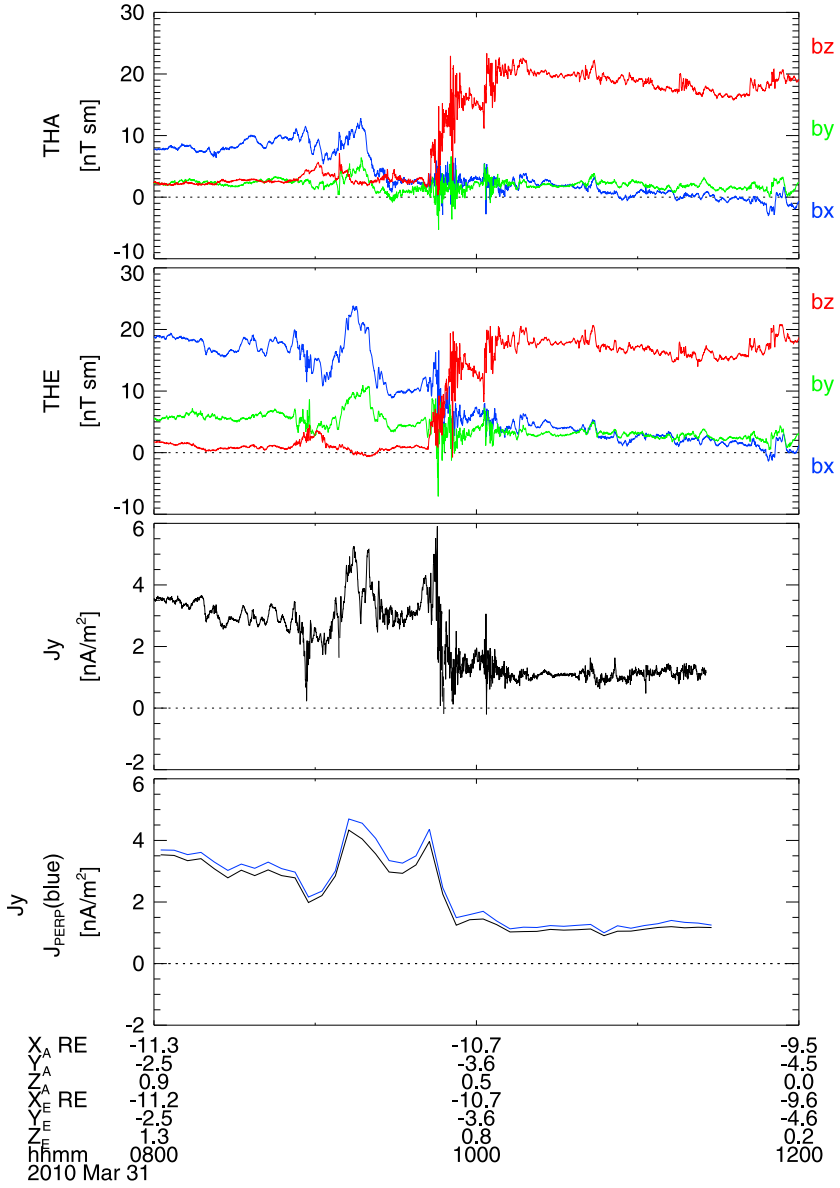

Figure A5. From top to bottom, (first and second panels) the THEMIS magnetometer data for 4 h. (third and fourth panels) The current densities calculated from the data from Figures A5 (first panel) and A5 (second panel). Figure A5 (third panel) represents 3 s data of J_y. Figure A5 (fourth panel) shows 5 min averaged data of both J_y and $J_\perp$. The event on 31 March 2010 is an example of high-current-density observations in a tail structure during substorm. The current density decreased after the onset of the substorm.

linearly to the x locations having tilt angles from 20° to 30° for dipole tilt angles >20°. However, the observed tilt was, at most, ~7.5° (~0.5 R_E/3 R_E), indicating that $Z = 0$ in SM coordinates corresponds relatively better with the plane of the magnetic equator and the central plane of the current sheet.

Appendix B: The Validity of J_y as the Cross-Tail Current Density

This study assumed that in the midnight sector of the tail, J_y can be suitably approximated by $\Delta B_x/\mu_0 \Delta z$ and can be regarded as the cross-tail current density. This appendix will show the validity of this assumption by demonstrating that (1) the amplitude of the field-aligned current is small in the y component and (2) the absolute value of $\Delta B_z/\mu_0 \Delta x$ is small for a dipolar structure. Using the same data set and the calculation criteria, J_x is $-\Delta B_y/\mu_0 \Delta z$. The field-aligned components are $J_{x\parallel} = J_x B_x/B$ and $J_{y\parallel} = J_y B_y/B$.

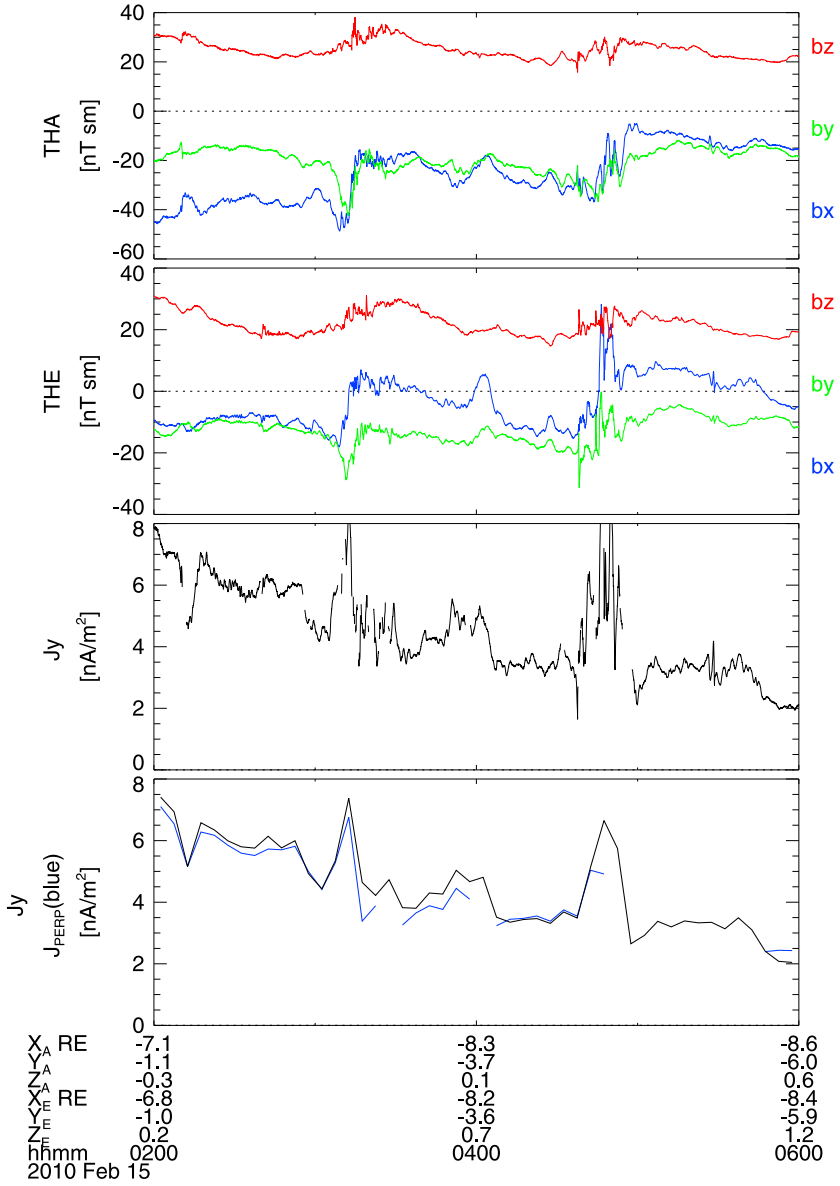

Figure A6. The plot format is the same as in Figure A5. This event on 15 February 2009 is another example of the high-current-density observations, but in a dipolar structure during substorm. As the spacecraft moved from a distance of 7.2 R_E at 0200 UT to 10.5 R_E at 0600 UT, J_y decreased gradually. Additionally, after the substorm onsets at 0300 and at 0430 UT, the current densities increased and the high current densities lasted for 10 to 15 min.

Figure A4 shows the relationship between the absolute values of J_y and the perpendicular component $J_\perp = \sqrt{(J_y - J_{y\parallel})^2 + (J_x - J_{x\parallel})^2}$. It is evident that most of the observed J_y values were almost identical to the $J_\perp$ values.

Figures A5 and A6 are 4 h plots of the high-current-density observations on 31 March 2010 and 15 February 2009, respectively. Figure A5 is consistent with the conventional picture of the current density evolution during the substorm growth phase. The current density was high before the substorm onset and decreased during the expansion phase. The high current density appeared in the tail structure. Figure A6 includes an interval of the high current density in the dipolar structure. For both events, J_y and $J_\perp$ were almost identical. The assumption of J_y as the cross-tail current density holds during substorms.

The absolute value of $\Delta B_z/\mu_0 \Delta x$ for a dipolar structure in the near-Earth tail can be estimated from Figure A6. On 15 February 2009, the THEMIS spacecraft moved from a distance of 7.2 R_E at 0200 UT to 10.5 R_E at 0600 UT. Meanwhile, J_y had decreased gradually, and B_z had not decreased, as expected from an ideal dipole. This observation suggests that the absolute value of $\Delta B_z/\mu_0 \Delta x$ for the dipolar structure is negligible in the near-Earth tail. In this region, the magnetic geometry is far from the ideal dipole geometry in a vacuum. (The term dipolar means that it is only relatively dipolar.)

Acknowledgments

We acknowledge NASA contract NAS5-02099 and V. Angelopoulos for allowing the use of data from the THEMIS Mission. Specifically, we thank K.H. Glassmeier, U. Auster, and W. Baumjohann for allowing the use of Fluxgate Magnetometer data provided under the lead of the Technical University of Braunschweig with financial support through the German Ministry for Economy and Technology and the German Center for Aviation and Space (DLR) under contract 50 OC 0302. The THEMIS, OMNI, and *AE* data were obtained through the THEMIS Data Analysis Software (http://themis.ssl.berkeley/edu/). We thank the Space Physics Data Facility at Goddard Space Flight Center (http://cdaweb.gsfc.nasa.gov) for the OMNI solar wind data and World Data Center for Geomagnetism (http://wdc.kugi.kyoto-u.ac.jp) for the *AE* index. All data and software listed above are open to public. Event lists obtained in this study are available from the author (miho.saito@me.com) on request. This work was supported by JSPS KAKENHI, grant 25004057. The author is grateful to T. Nagai for improving the analysis. The author is also grateful to both reviewers for improving the manuscript.

Michael Liemohn thanks two anonymous reviewers for their assistance in evaluating this paper.

References

Akasofu, S.-I. (2013), Where is the magnetic energy for the expansion phase of auroral substorms accumulated?, *J. Geophys. Res. Space Physics*, *118*, 7219–7225, doi:10.1002/2013JA019042.

Akasofu, S.-I., A. T. Y. Lui, and C.-I. Meng (2010), The importance of auroral features in the search for substorm onset process, *J. Geophys. Res.*, *115*, A08218, doi:10.1029/2009JA014960.

Angelopoulos, V. (2008), The THEMIS mission, *Space Sci. Rev.*, *141*, 5–34, doi:10.1007/s11214-008-9336-1.

Asano, Y., R. Nakamura, W. Baumjohann, A. Runov, Z. Vörös, M. Volwerk, T. L. Zhang, A. Balogh, B. Klecker, and H. Rème (2005), How typical are atypical current sheets?, *Geophys. Res. Lett.*, *32*, L03108, doi:10.1029/2004GL021834.

Auster, H. U., et al. (2008), The THEMIS fluxgate magnetometer, *Space Sci. Rev.*, *141*, 235–264, doi:10.1007/s11214-008-9365-9.

Büchner, J., and L. M. Zelenyi (1989), Regular and chaotic charged particle motion in magnetotaillike field reversals: 1. Basic theory of trapped motion, *J. Geophys. Res.*, *94*, 11,821–11,842, doi:10.1029/JA094iA09p11821.

Cheng, C. Z. (1992), Magnetospheric equilibrium with anisotropic pressure, *J. Geophys. Res.*, *97*(A2), 1497–1510, doi:10.1029/91JA02433.

Donovan, E., et al. (2008), Simultaneous THEMIS in situ and auroral observations of a small substorm, *Geophys. Res. Lett.*, *35*, L17S18, doi:10.1029/2008GL033794.

Delcourt, D. C., H. V. Malova, and L. M. Zelenyi (2004), Dynamics of charged particles in bifurcated current sheets: The $\kappa \approx 1$ regime, *J. Geophys. Res.*, *109*, A01222, doi:10.1029/2003JA010167.

Delcourt, D. C., H. V. Malova, and L. M. Zelenyi (2006), Quasi-adiabaticity in bifurcated current sheets, *Geophys. Res. Lett.*, *33*, L06106, doi:10.1029/2005GL025463.

Génot, V., F. Mottez, G. Frui, P. Louarn, J.-A. Sauvaud, and A. Balogh (2005), Bifurcated current sheet: Model and Cluster observations, *Planet. Space Sci.*, *53*, 229–235.

Greco, A., A. L. Taktakishvili, G. Zimbardo, P. Veltri, and L. M. Zelenyi (2002), Ion dynamics in the near-Earth magnetotail: Magnetic turbulence versus normal component of the average magnetic field, *J. Geophys. Res.*, *107*(A10), 1267, doi:10.1029/2002JA009270.

Hoshino, M., A. Nishida, T. Mukai, Y. Saito, T. Yamamoto, and S. Kokubun (1996), Structure of plasma sheet in magnetotail: Double-peaked electric current sheet, *J. Geophys. Res.*, *101*(A11), 24,775–24,786, doi:10.1029/96JA02313.

Hsieh, M.-S., and A. Otto (2014), The influence of magnetic flux depletion on the magnetotail and auroral morphology during the substorm growth phase, *J. Geophys. Res. Space Physics*, *119*, 3430–3443, doi:10.1002/2013JA019459.

Ohtani, S., K. Takahashi, L. J. Zanetti, T. A. Potemra, R. W. McEntire, and T. Iijima (1992), Initial signatures of magnetic field and energetic particle fluxes at tail reconfiguration: Explosive growth phase, *J. Geophys. Res.*, *97*(A12), 19,311–19,324, doi:10.1029/92JA01832.

Petrukovich, A. A., A. V. Artemyev, H. V. Malova, V. Y. Popov, R. Nakamura, and L. M. Zelenyi (2011), Embedded current sheets in the Earth's magnetotail, *J. Geophys. Res.*, *116*, A00I25, doi:10.1029/2010JA015749.

Ricci, P., G. Lapenta, and J. U. Brackbill (2004), Structure of the magnetotail current: Kinetic simulation and comparison with satellite observations, *Geophys. Res. Lett.*, *31*, L06801, doi:10.1029/2003GL019207.

Matsui, T., and W. Daughton (2008), Kinetic theory and simulation of collisionless tearing in bifurcated current sheet, *Phys. Plasma*, *15*, 012901.

Mitchell, D. G., D. J. Williams, C. Y. Huang, L. A. Frank, and C. T. Russell (1990), Current carriers in the near-Earth cross-tail current sheet during substorm growth phase, *Geophys. Res. Lett.*, *17*(5), 583–586, doi:10.1029/GL017i005p00583.

Nagai, T., T. Mukai, T. Yamamoto, A. Nishida, S. Kokubun, and R. P. Lepping (1997), Plasma sheet pressure changes during the substorm growth phase, *Geophys. Res. Lett.*, *24*(8), 963–966, doi:10.1029/97GL00374.

Narita, Y., R. Nakamura, and W. Baumjohann (2013), Cluster as current sheet surveyor in the magnetotail, *Ann. Geophys.*, *31*, 1605–1610, doi:10.5194/angeo-31-1605-2013.

Runov, A., R. Nakamura, W. Baumjohann, T. L. Zhang, M. Volwerk, H.-U. Eichelberger, and A. Balogh (2003), Cluster observation of a bifurcated current sheet, *Geophys. Res. Lett.*, *30*(2), 1036, doi:10.1029/2002GL016136.

Saito, M. H., Y. Miyashita, M. Fujimoto, I. Shinohara, Y. Saito, K. Liou, and T. Mukai (2008), Ballooning mode waves prior to substorm-associated dipolarizations: Geotail observations, *Geophys. Res. Lett.*, *35*, L07103, doi:10.1029/2008GL033269.

Saito, M. H., D. Fairfield, G. Le, L.-N. Hau, V. Angelopoulos, J. P. McFadden, U. Auster, J. W. Bonnell, and D. Larson (2011), Structure, force balance, and evolution of incompressible cross-tail current sheet thinning, *J. Geophys. Res.*, *116*, A10217, doi:10.1029/2011JA016654.

Sergeev, V., Y. Nishimura, M. Kubyshkina, V. Angelopoulos, R. Nakamura, and H. Singer (2012), Magnetospheric location of the equatorward prebreakup arc, *J. Geophys. Res.*, *117*, A01212, doi:10.1029/2011JA017154.

Sergeev, V. A., D. G. Mitchell, C. T. Russell, and D. J. Williams (1993), Structure of the tail plasma/current sheet at ~11 R_E and its changes in the course of a substorm, *J. Geophys. Res.*, *98*(A10), 17,345–17,365, doi:10.1029/93JA01151.

Sergeev, V., et al. (2003), Current sheet flapping motion and structure observed by Cluster, *Geophys. Res. Lett.*, *30*(6), 1327, doi:10.1029/2002GL016500.

Sitnov, M. I., et al. (2003), A model of the bifurcated current sheet, *Geophys. Res. Lett.*, *30*(13), 1712, doi:10.1029/2003GL017218.

Snekvik, K., E. Tanskanen, N. Østgaard, L. Juusola, K. Laundal, E. I. Gordeev, and A. L. Borg (2012), Changes in the magnetotail configuration before near-Earth reconnection, *J. Geophys. Res.*, *117*, A02219, doi:10.1029/2011JA017040.

Tang, C.-L., L. Li, Z.-Y. Li, and Z.-X. Liu (2006), Bifurcated current sheet structure in quiet time by Cluster spacecraft, *Chin. Phys. Lett.*, *23*(4), 1054–1056.

Thompson, S. M., M. G. Kivelson, M. El-Alaoui, A. Balogh, H. Réme, and L. M. Kistler (2006), Bifurcated current sheets: Statistics from Cluster magnetometer measurements, *J. Geophys. Res.*, *111*, A03212, doi:10.1029/2005JA011009.

Tsyganenko, N. A., S. B. P. Karlsson, S. Kokubun, T. Yamamoto, A. J. Lazarus, K. W. Ogilvie, C. T. Russell, and J. A. Slavin (1998), Global configuration of the magnetotail current sheet as derived from Geotail, Wind, IMP 8 and ISEE 1/2 data, *J. Geophys. Res.*, *103*(A4), 6827–6841, doi:10.1029/97JA03621.

Zelenyi, L. M., D. C. Delcourt, H. V. Malova, and A. S. Sharma (2002), "Aging" of the magnetotail thin current sheets, *Geophys. Res. Lett.*, *29*(12), 1608, doi:10.1029/2001GL013789.